1976-12-01

Analysis of the voltage drop arising from a collision-dominated sheath

Dolson, R.C.; Biblarz, O.

American Institute of Physics

Journal Name: J. Appl. Phys.; (United States); Journal Volume: 47:12
http://hdl.handle.net/10945/60969

Analysis of the voltage drop arising from a collision-dominated sheath

R. C. Dolson* and O. Biblarz

Department of Aeronautics, Naval Postgraduate School, Monterey, California 93940
(Received 22 March 1976)

Voltage drops associated with the collisional sheath of nonemitting, MHD electrodes are investigated. The problem is described by a set of coupled nonlinear partial differential equations which are solved by finite differencing in a computer. The sheath and ambipolar regions form in a self-consistent way obviating the need to match boundaries. A two-dimensional model with periodic active sites on a flat plate is used. The current constricts at these sites in order to satisfy the controlling equations for frozen charge flow. The effects of a magnetic field as well as of Joule heating are included in the model; convection can be shown to be negligible in the sheath. Joule heating is assumed to have no effect on the bulk temperature of the gas. Changes in the current-voltage characteristics due to Joule heating are small since the effect is extremely localized; the presence of a magnetic field has a slight influence on the size of the sheath but alters noticeably the current-voltage characteristics.

PACS numbers: 52.40.Kh, 52.30.+r, 52.75.Fk

I. INTRODUCTION

The principal voltage-consuming mechanisms in a flowing collision-dominated plasma can be divided into two main classes, boundary-layer and sheath drops. In an MHD generator, these drops correspond to internal voltage losses. Boundary-layer drops are those that occur because of the finite conductivity of a real plasma, coupled with the existence of thermal boundary layers near electrode surfaces. Sheath drops occur as the result of Debye shielding, a non-neutral layer which forms adjacent to an electrode and results in a space-charge electric field.

Although the existence of a collisional sheath at an electrode surface is well understood, its effect on MHD-generator voltage losses has been investigated to a much lesser extent than those of the boundary layer. This is principally because the sheath is described by a relatively complicated set of coupled nonlinear partial differential equations.[1-3] Some authors[4] assign a negligible value to the sheath voltage drop relative to the boundary-layer losses on the basis of the classical Langmuir probe theory. In our work, the sheath is considered collisional and, as will be shown, there can be a significant voltage drop associated with it. The study of a collisional sheath is warranted since the extent of the sheath in combustion MHD generators as well as in many other plasma devices is greater than the electron mean free path; moreover, collisionless probe analyses can explain neither substantial voltage drops nor current constrictions at the anode.[5] It should be noted that if convection is negligible in the sheath then the contributions of the sheath and of the boundary layer may be computed separately.

Because the sheath and ambipolar regions can be very small compared to the size of the electrode, at first glance the problem appears to be one-dimensional except at the edges. No one-dimensional solution exists, however, for the frozen flow of charges through a collisional sheath[5] since a Cartesian geometry in one dimension is devoid of the necessary geometric decrease of current density away from the electrode. This density decrease is inherent with cylindrical or spherical geometries. Because current must constrict towards the electrode, a two-dimensional model is proposed which represents a flat plate anode with periodic active sites or nodes through which current flows (see Fig. 1). It must be pointed out that this paper does not address the problem of arc constrictions associated with thermal instabilities,[6] but rather geometric constrictions required to satisfy charge conservation and Ohm's law.

By modeling a flat plate electrode with periodic miniscule wire electrodes, where the region between wires is treated as an insulated wall, it is possible to restrict the computational field to one such site as shown in Fig. 2. The electrode node represents the active site where current flows. Node spacing would in practice be dictated by surface irregularities, seed deposits, etc., which are known to be random and difficult to describe. But it is important to note that the minimum node spacing is determined by the requirements for two-dimensional current flow within the sheath. The characteristic sheath length appears to be a minimum spacing for the active sites, since further crowding would cause the sheath regions of adjacent nodes to overlap. This would precipitate the same situation which causes the one-dimensional solution not to exist.[5] Calculations presented in this work use a near-maximum node concentration, resulting in a minimum voltage drop for a given current density. The undisturbed plasma or free stream boundary can be shown to be imbedded well within an existing boundary layer. This boundary represents the region of

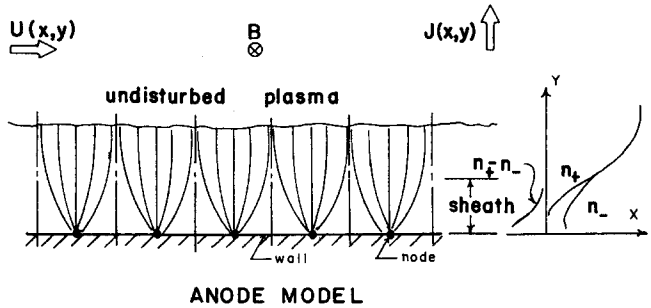

ANODE MODEL

FIG. 1. Anode model with periodic current constriction.

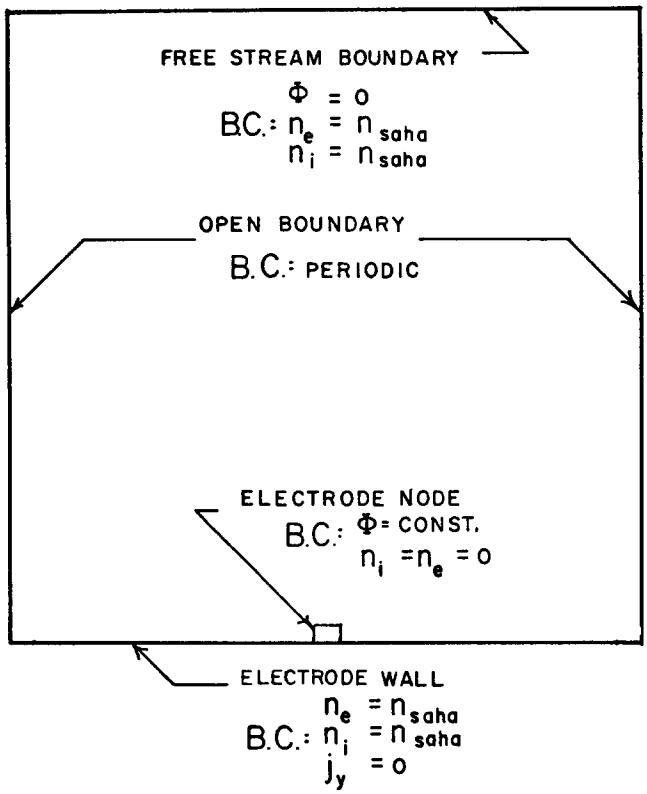

FIG. 2. Arrangement of electrode and boundary conditions for computational array.

charge neutrality and local equilibrium which exists beyond the ambipolar region.

The field is modeled in the computer with grid points which contain elements of finite-differenced versions of the controlling equations. Results presented in this paper are derived from a 51×51 point grid representing a domain whose size is three to four sheath lengths on a side. The computer solution involves solving the species equations and Poisson's equation simultaneously in a line-iterative fashion in order to reduce storage requirements. The energy equation is solved externally to the others with each iteration. The species equations, shown in Sec. II, present special programming problems because they contain mostly nonlinear terms. One solution procedure in such cases is to include all nonlinear terms on the "right-hand side", that is, external to the coefficient matrix, in the hope that they change slowly enough with each iteration to render a convergent iterative process. This procedure is known as the Jacobi method.[7] The species equations are not suited for such a procedure since there is only one linear term in each of the two equations and there is no prescribed "load" to the system. As a consequence a quasi-Jacobi method is used: When the product of two variables is encountered, one variable is treated as a constant coefficient of the other for each iteration. This means that the nonlinear terms are retained in the coefficient matrix. The "constant" coefficients are updated after every iteration, thus changing the coefficient matrix. Although a three-dimensional node model would be more realistic, the two-dimensional quasi-Jacobi program is already taxing the IBM 360-67 machine capability.

II. FORMULATION

The following assumtions are used within the disturbed plasma region: (1) Steady state, (2) frozen composition, (3) no ion emission from the anode, (4) no continuum radiation losses in the energy equation, (5) negligible convection, and (6) negligible ion current density at the free stream boundary.

To determine the significance of ionization and recombination in the formation of the sheath, a comparison of characteristic lengths must be made. Using a fractional analysis[8,9] on Poisson's equation to determine the thickness of the sheath, one obtains

$$\lambda_s \approx (\phi\epsilon_0/en)^{1/2}, \tag{1}$$

with the variable defined in Sec. VI. At a temperature of 2000 °K, a typical MHD plasma has a charged particle density of about 10^{18} particles/m^3. When the potential drop is 10 V, Eq. (1) gives a sheath length of 2.4×10^{-5} m. From Hinnov and Hirschberg[5,10] the three-body recombination length is given by

$$\frac{dn_e}{dt} = \alpha n_e^2, \tag{2}$$

where

$$\alpha = 5.6\times10^{-39}(kt/e)^{-4.5}n_e. \tag{3}$$

Using the same values as above, the characteristic recombination time τ_r amounts to 6.5×10^{-2} sec. This time corresponds to a "recombination mean free path" of about 1 mm (Ref. 10, p. 149) for the conditions stated and longer paths for lower temperatures. That is, the average distance traveled by an ion before it recombines is about 100 times bigger than the extent of the sheath which is an indication of the low probability of recombination. Although it does not necessarily follow, we shall assume that ionization is negligible in the sheath as well. If the ambipolar region is of the same order as the sheath length, ionization/recombination is not expected to play a part in that region either. As the voltage increases, the ambipolar region grows and may even become of the order of the boundary-layer thickness, in which case recombination and convection would not be negligible. But voltage drops associated with the ambipolar region are small compared to the sheath and no significant errors are introduced by ignoring the growth of the ambipolar region. The boundary-layer calculation would account for the Ohmic contribution.

It is relatively simple to show that convective effects have little or no direct influence on the electron sheath. Note first that the size of the sheath is typically less than one hundredth that of the boundary layer. If we take the speed of sound as characteristic for the core flow and use a $\frac{1}{7}$th turbulent profile, the convective velocity turns out to be about 400 m/sec at the sheath's outer edge. Now, the minimum electron velocity in the sheath is the corresponding thermal velocity which is about 10^5 m/sec. It may be stated, therefore, that convection will not have any direct effect in the behavior of the anode sheath for plasmas operating at pressures of around 1 atm.

The governing equations used are introduced below. The generalized Ohm's law is written[11]

$$\mathbf{J}_s = -e\mu_s n_s \nabla\phi - (\beta_s/|B|)(J_s\times B) \pm eD_s\nabla n_s, \tag{4}$$

where the subscript "s" refers to electrons or ions and the + and − signs preceding the diffusion terms apply to the electron and ion current, respectively. Species continuity is given by

$$\nabla \cdot \mathbf{J}_s = 0. \tag{5}$$

Poisson's equation is

$$\nabla^2 \phi + (e/\epsilon_0)(n_i - n_e) = 0. \tag{6}$$

Einstein's relation is of the form

$$D_s/\mu_s = kT_s/e. \tag{7}$$

Finally, in a quiescent plasma an expression accounting for the electron energy balance is[11]

$$\mathbf{J}_e \cdot \nabla \phi = 3 n_e k (T - T_e) \sum_n \nu_{en} \delta_n m_e/m_n. \tag{8}$$

A more useful form of the governing equations is obtained through dimensional analysis.[12] Such an alaysis generates the following intrinsic nondimensional variables:

$$\hat{n}_i = n_i/n_0, \quad \hat{n}_e = n_e/n_0, \quad \hat{\phi} = \phi/\phi_0, \quad \hat{\nabla} = L\nabla$$
$$\hat{x} = x/L, \quad \hat{y} = y/L, \quad \theta = T_e/T_0,$$

where the characteristic parameters are

$$\phi_0 \equiv kT_0/e, \quad L \equiv e^2/\epsilon_0 k T_0, \quad \text{and } n_0 \equiv (kT_0\epsilon_0/e^2)^3.$$

T_0 is the bulk temperature which is considered to be constant and independent of Joule heating, i.e., the system is thermally stable. This assumption is consistent with low levels of Joule heating because the electrode, usually a good thermal conductor, has a strong stabilizing influence on the gas temperature. Note that the ratio of the characteristic length L to the Debye length turns out to be $\hat{n}_e^{1/2}$. The fact that $n_0 = L^{-3}$ is of no fundamental significance; this equality can be easily avoided by defining $\rho = en$ as the dependent variable.

The energy equation requires additional consideration. A parameter γ, which is a measure of the degree of Joule heating, has the following nondimensional form:

$$\gamma \equiv \frac{0.13(kT_0)^4 \epsilon_0^2 m_n}{P_0^2 Q_{en}^2 m_e \delta_n e^4 (1+\beta^2)}. \tag{9}$$

Equation (9) is a collection of terms whose value is dictated by the chemical constituents of the plasma as well as the pressure, free stream temperature, and Hall parameter. Inherent in its derivation are the assumptions[13] that the collision frequency varies as $\theta^{1/2}$ and that the electron mobility varies as $\theta^{-1/2}$. The value $\gamma = 0$ represents no Joule heating. A typical MHD plasma consisting of combustion products would have $\gamma \approx 100$, while argon with cesium seed would have $\gamma \approx 10^6$.

Combining the current equation with continuity, Einstein's relation, and Poisson's equation yields the two species equations which in nondimensional form are

$$\theta \hat{n}_e(\hat{n}_i - \hat{n}_e) - \theta \hat{\nabla}\hat{n}_e \cdot \hat{\nabla}\hat{\theta} + \tfrac{1}{2}\hat{n}_e \hat{\nabla}\hat{\phi} \cdot \hat{\nabla}\hat{\theta} + \theta^2 \hat{\nabla}^2 n_e + \tfrac{1}{2}\theta \hat{\nabla}\theta \cdot \hat{\nabla}\hat{n}_e$$
$$+ \beta \left(-\tfrac{1}{2}\hat{n}_e \frac{\partial \hat{\phi}}{\partial \hat{y}} \frac{\partial \theta}{\partial \hat{x}} + \tfrac{1}{2} n_e \frac{\partial \hat{\phi}}{\partial \hat{x}} \frac{\partial \theta}{\partial \hat{y}} + \theta \frac{\partial \hat{\phi}}{\partial \hat{y}} \frac{\partial \hat{n}_e}{\partial \hat{x}} - \theta \frac{\partial \hat{\phi}}{\partial \hat{x}} \frac{\partial \hat{n}_e}{\partial \hat{y}} \right.$$
$$\left. - \tfrac{1}{2}\theta \frac{\partial \theta}{\partial \hat{x}} \frac{\partial \hat{n}_e}{\partial \hat{y}} + \tfrac{1}{2}\theta \frac{\partial \theta}{\partial \hat{y}} \frac{\partial \hat{n}_e}{\partial \hat{x}} \right) = 0 \tag{10}$$

and

$$\hat{n}_i(\hat{n}_i - \hat{n}_e) - \hat{\nabla}\hat{n}_i \cdot \hat{\nabla}\hat{\phi} - \hat{\nabla}^2 \hat{n}_i = 0. \tag{11}$$

The nondimensional Poisson's equation is

$$\hat{\nabla}^2 \hat{\phi} + \hat{n}_i - \hat{n}_e = 0. \tag{12}$$

Finally, the energy equation reads

$$\gamma \hat{J}_e \cdot \hat{\nabla}\hat{\phi} = -\hat{n}_e(\theta^2 - \theta). \tag{13}$$

The boundary conditions are indicated in Fig. 2. The electrode node is catalytic and has a given potential relative to the free stream. The "insulated wall" equilibrates the charges and allows no perpendicular current. Upstream and downstream boundaries are periodic. At the free stream boundary we assume equilibrium charge densities and $\theta = 1$; at solid surfaces we also assume $\theta = 1$. It may be pointed out that the set of equations, i.e., Eqs. 10–12, accepts only certain boundary conditions. In particular, an attempt to model a catalytic insulated wall failed to render meaningful answers.

III. RESULTS

Figures 3 and 4 show profiles for two nondimensional potentials along a cut perpendicular to the electrode wall passing through the active site. These two computer runs excluded magnetic and Joule heating effects. The array size refers to the length of the over-all field; y is given in terms of the characteristic length L defined earlier. The sheath and the ambipolar region are evident in these figures. At 2000 °K, the total length across the field is $500L$ which corresponds to 5.3×10^{-5} m, whereas the length of $1000L$ corresponds to 10.6×10^{-5} m.

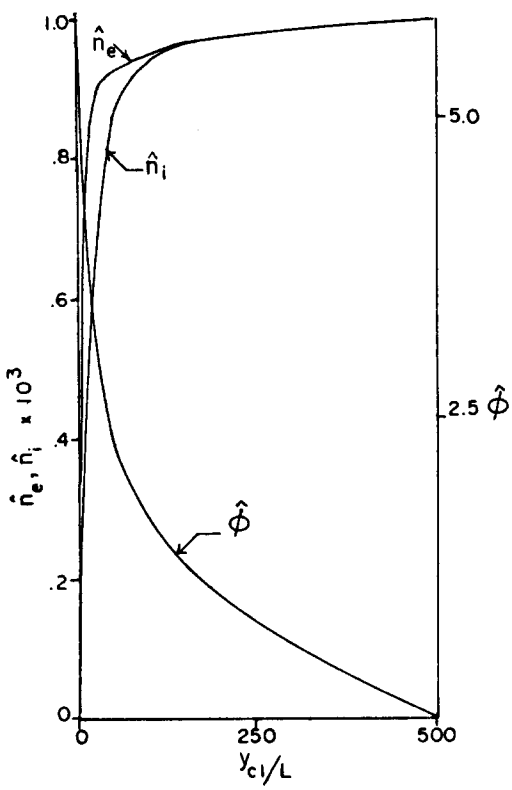

FIG. 3. Potential and charge density profiles, $\hat{\phi} = 5.80$, $\gamma = 0$, $\beta = 0$, $\hat{n} = 10^{-3}$, array size = $500L$.

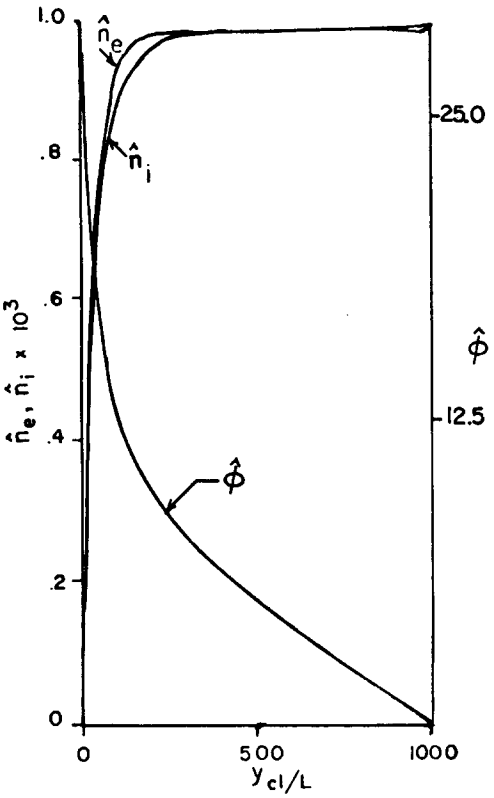

FIG. 4. Potential and charge density profiles, $\hat{\phi}=29.0$, $\gamma=0$, $\beta=0$, $\hat{n}=10^{-3}$, array size $=1000L$.

For the higher potential (Fig. 4) the $500L$ field would not have been large enough to include all of the ambipolar region. Doubling the array size to include all of the sheath and ambipolar region also doubles the node spacing which makes comparison of several voltages cumbersome. For better comparison when the array size was doubled two active periodic sites were used for some

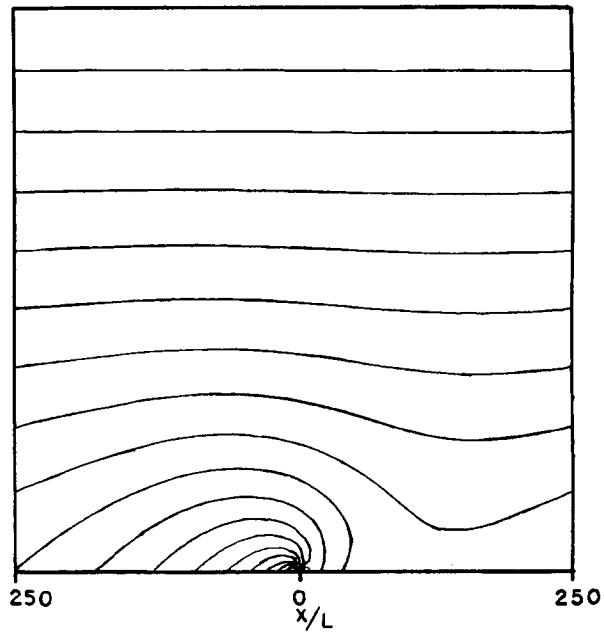

FIG. 6. Potential contour plot, $\hat{\phi}=29.0$, $\gamma=0$, $\beta=1$, $\hat{n}=10^{-3}$, array size $=500L$.

runs resulting in the same electric node width. Due to the instabilities of the nonlinear equation finite-difference formulation, there is a limit to the size of the field that the array can represent for a given potential. There is also an upper limit on the potential and magnetic field values that can be used for a given array.

At a temperature of 2000 °K the characteristic parameters ϕ_0 and n_0 are 0.172 and 8.64×10^{20}, respectively. In Fig. 4, $\hat{\phi}=29.0$ and $\hat{n}=10^{-3}$. These represent a potential of 5.80 V and a charge density of 8.64×10^{17} particles/m^3, respectively. From Eq. 1, the predicted sheath length is 1.79×10^{-5}m; the sheath length in Fig. 4

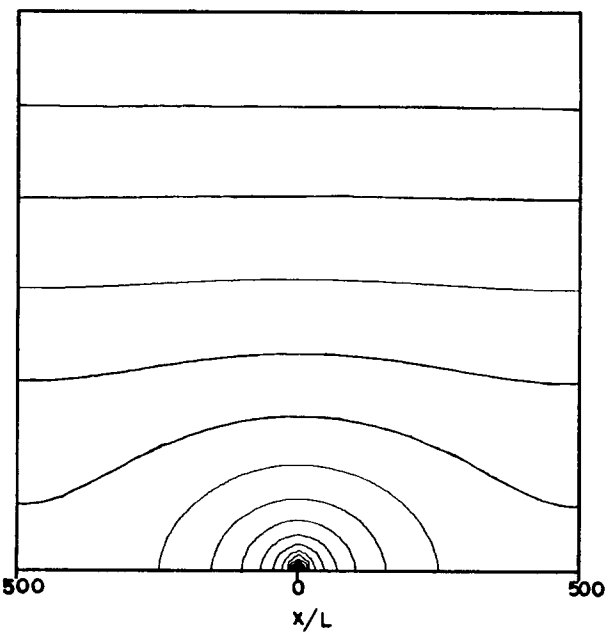

FIG. 5. Potential contour plot, $\hat{\phi}=29.0$, $\gamma=0$, $\beta=0$, $\hat{n}=10^{-3}$, array size $=1000L$.

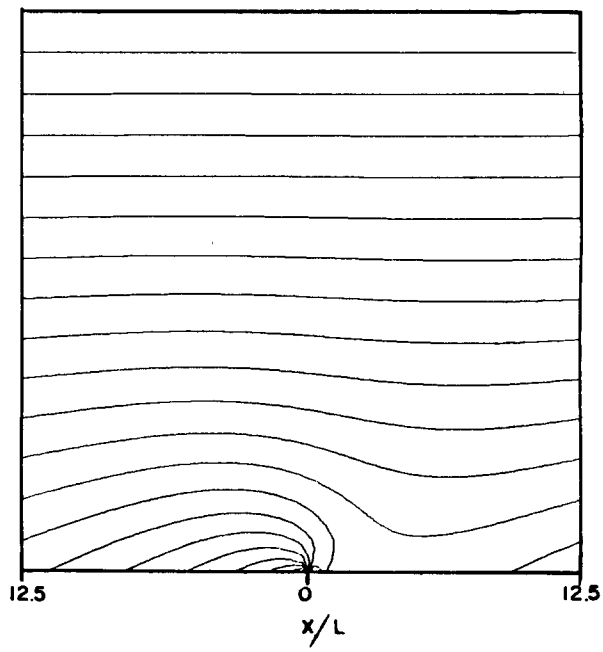

FIG. 7. Potential contour plot, $\hat{\phi}=5.80$, $\gamma=0$, $\beta=2$, $\hat{n}=1$, array size $=25L$.

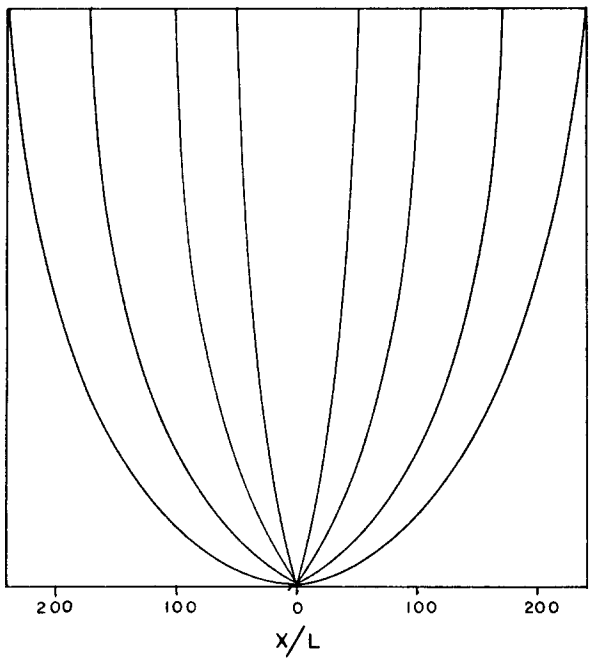

FIG. 8. Current density contour plot, $\hat{\phi}=5.80$, $\gamma=0$, $\beta=1$, $\hat{n}=10^{-3}$, array size $=500L$.

is about $350L$ or 3.68×10^{-5} m. The length predicted by the fractional analysis and that from the computer calculation are therefore of the same order of magnitude. Furthermore, it can be seen that this length is small compared to the extent of the usual boundary layer and thus convection may be ignored in the sheath.

Figure 5 is a typical contour plot of the potential in the field for a case with no Joule heating or magnetic field. The coordinate x is also given in terms of L. Figures 6 and 7 show what happens when a Hall parameter greater than zero is used. There is little visible change to the

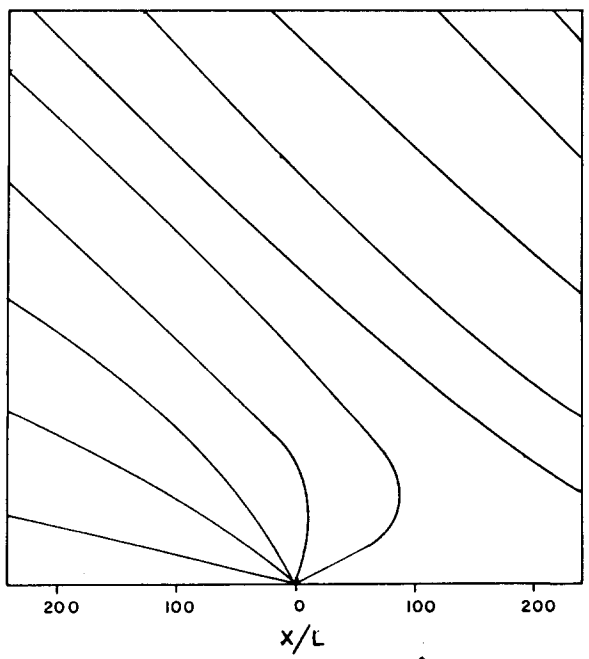

FIG. 9. Current density contour plot, $\hat{\phi}=5.80$, $\gamma=0$, $\beta=1$, $\hat{n}=10^{-3}$, array size $=500L$.

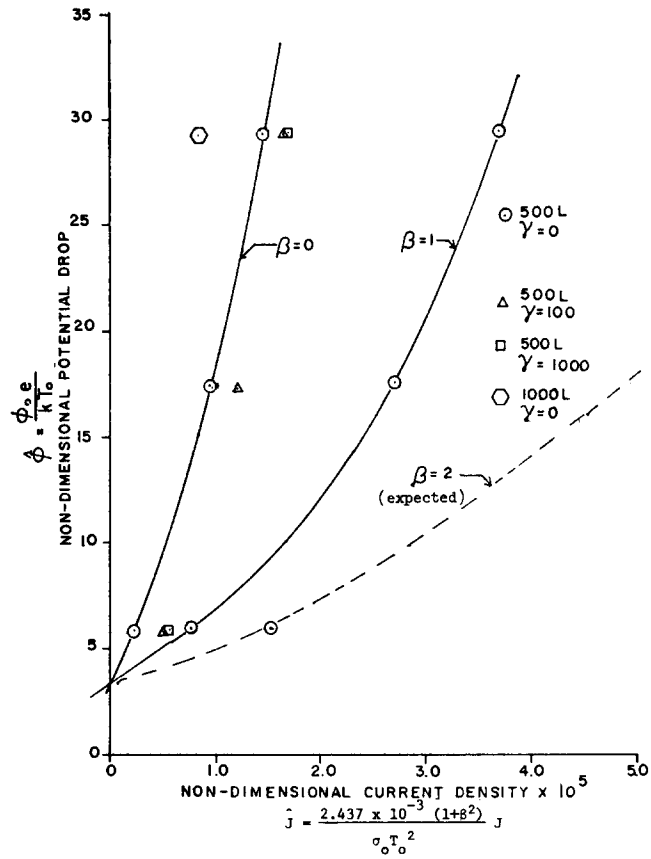

FIG. 10. Current-voltage diagram, $\hat{n}=10^{-3}$.

plots with the introduction of Joule heating so they are not presented here. The effect of Joule heating on the current is discussed later.

Current streamlines are shown in Figs. 8 and 9 for Hall parameters of 0 and 1, respectively. As can be predicted from the equations, the current lines make an

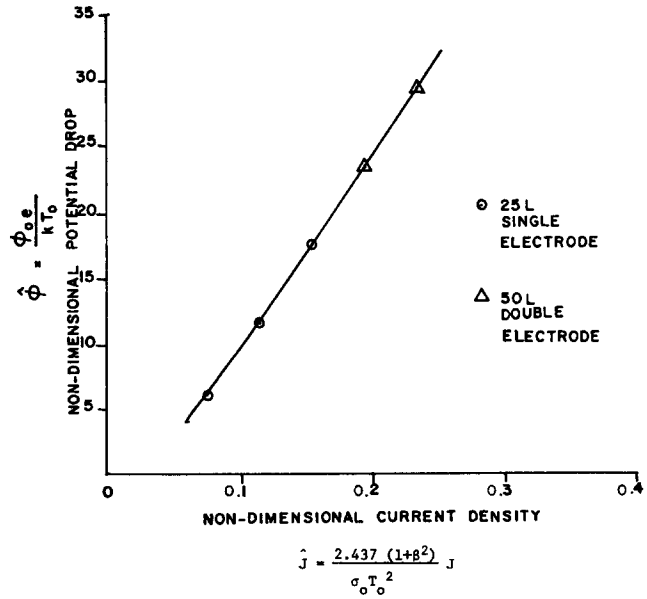

FIG. 11. Current-voltage diagram, $\hat{n}=1.0$, $\beta=0$, 41×41 grid.

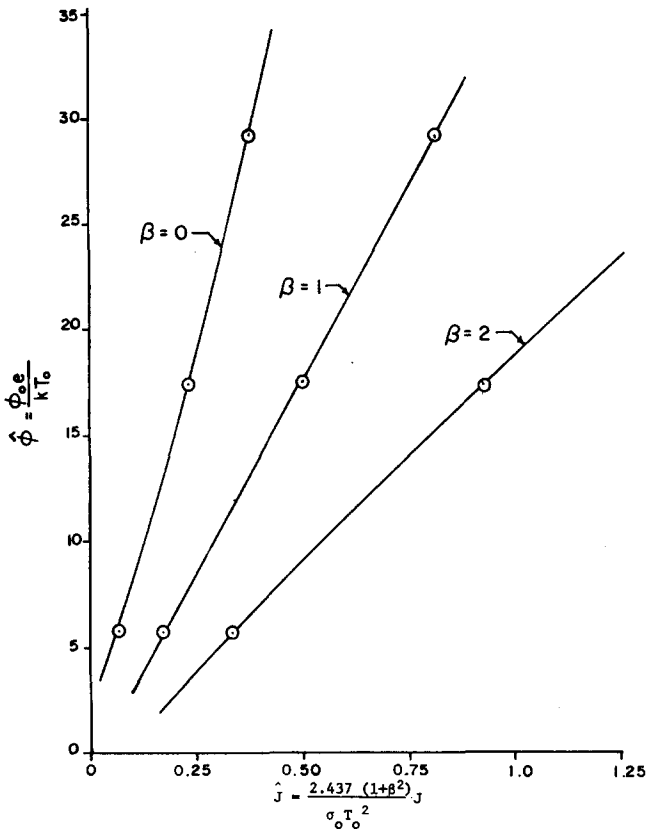

FIG. 12. Current-voltage diagram, $\hat{n}=1.0$, 51×51 grid.

angle with the potential contour lines approximately equal to the Hall angle and would be exact except for the effects of diffusion which only affect the immediate vicinity of the electrode.

Figures 10—12 are current-voltage plots. The current density has been nondimensionalized consistent with the intrinsic parameters, but a *local* conductivity replaces the mobility to make the graph easier to use. Constant terms were collected to give the simplified coefficient shown in the figures. Since numerical instabilities prevent the calculation of larger potentials for the grid size shown, the curves must be extrapolated to make them usable for a wider range of current densities.

In the absence of a magnetic field the space-charge current-voltage diagrams tend to be concave upward, a fact that can be predicted[13] from the proportionality $J\alpha\phi^2/y^3$ for a high-pressure plasma. If y is taken as the sheath length λ_s, it can be shown that ϕ varies as J^2.

Figure 10 shows the effect of the introduction of Joule heating on the current-voltage characteristics. There tends to be an increase in the current density for a given potential drop across the sheath. This seems reasonable since the conductivity increases with increasing electron temperature. The effect of Joule heating on current density is, however, limited since, as shown in Fig. 13, the electron temperature increase is highly localized. It is interesting to note theat in spite of the limited effect of Joule heating on the results, it had a definite stabilizing effect on the numerical process and reduced the time to convergence dramatically.

Figure 11 shows what happens when two periodic nodes are introduced into the calculation field. For the double-node cases, the characteristic field size is also doubled, giving the same effective width between nodes. If the array size had been doubled without introducing a second electrode, the current density would have been cut in half for those voltages.

Figure 12 is the current-voltage diagram for the case $\hat{n}=1$ and various Hall parameters. From observation, the current densities at $\beta=2$ are about twice that at $\beta=1$. Since no stable solution was achieved for $\beta=2$ and $\hat{n}=10^{-3}$, the above results were used to sketch the "expected" line for $\beta=2$ in Fig. 10.

IV. COMPARISONS WITH EXPERIMENT

Argyropoulos *et al.*[4] cite the use of a sophisticated computer solution for the boundary-layer drop calculation of conditions relevant to the AVCO-APL channel. Their results show the anode drop to be 101 V due to the boundary layer. They do not consider any sheath effects. Using these data, namely, $T_{elec}=2000\,^{\circ}\mathrm{K}$, $J=3.95\times10^4$ A/m^2, $\beta=1.02$, and a chemistry consisting of toluene and oxygen with cesium seed, the equilibrium conductivity at the electrode is 1.14 mho/m. The corresponding nondimensional current density is 4.307×10^{-5}. Taking the $\beta=1$ line in Fig. 10 gives $\hat{\phi}=35.6$, or an actual anode sheath drop of 6.13 V at the given temperature. The measurements appear to represent about 130 V for the anode drops.

Another comparison is from the work of Sonju and Teno.[14] For this experiment they used the same chemical constituents as in the AVCO-APL channel. The conductivity at the wall temperature of 1800 °K is 0.30 mho/m, other parameters are $J=1.6\times10^4$ A/m^2 and $\beta=1.8$. Figure 10 gives $\hat{J}=1.7\times10^{-4}$, $\phi=121.3$, which

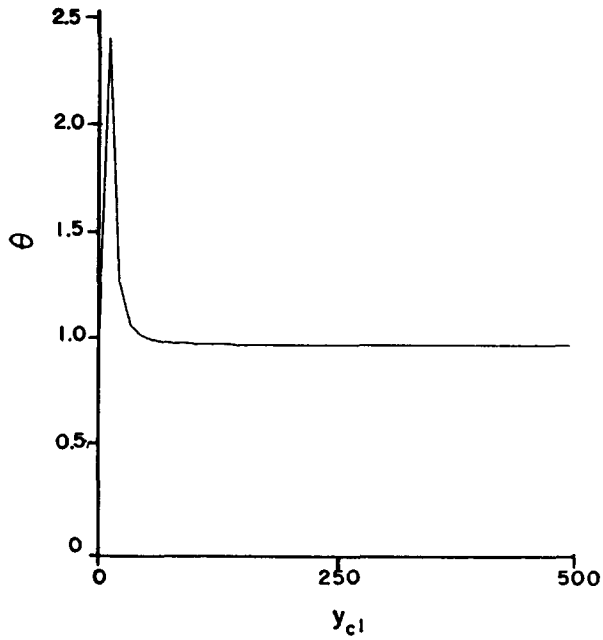

FIG. 13. Electron temperature profile, $\hat{\phi}=5.80$, $\gamma=100$, $\beta=0$, $\hat{n}=10^{-3}$, array size $=500L$.

translates to an anode sheath voltage drop of 18.8 V. The total drop at the anode measured was about 150 V.

Caution must be exercised when making these comparisons since several factors have not been considered. First, any degree of nonequilibrium would increase the conductivity near the electrode resulting in a smaller potential drop. Second, nothing has been said about the node density of the experiments as compared to the assumptions made in our numerical solutions (where the distance between nodes is of the order of the sheath length). Should the actual node density differ from this, it will affect the current-voltage characteristics. Third, the use of a two-dimensional model rather than a three-dimensional one may tend to overpredict voltage drops. The following example illustrates these limitations. An experiment by Kessler and Eustis[15] was conducted using ethanol in oxygen with 1% KOH. Nitrogen was introduced for cooling such that the N_2/O_2 ratio was 0.5. For this run, $T_{elec}=1685\,^{\circ}\mathrm{K}$, $J=0.75\times10^{4}\ \mathrm{A/m^2}$, $\beta=1.5$, and the electrode conductivity is 0.056 mho/m. Figure 10 gives for $\hat{J}=3.697\times10^{-4}$, $\hat{\phi}=490.2$ or $\phi=71.1$ V. This is a somewhat higher drop than the measured 45 V that should account for both the sheath and boundary-layer contributions.

The primary difference between the above examples appears to be the conductivity at the electrodes. Since the equilibrium conductivity has such a strong dependence on temperature, the electrode temperature is a critical parameter in controlling the sheath losses. A very accurate comparison can only be made using a plot generated from the correct charge density and on precise knowledge of anode temperatures.

It is common practice to predict the losses according to the empirical formula

$$V=A+B\delta, \tag{14}$$

where δ is the boundary-layer thickness and A and B are constants determined for a particular experiment. Such a scheme might be useful here if A is the sheath drop and $B\delta$ is the boundary-layer drop. For the Argyropoulus example, Ref. 4 predicts a boundary-layer drop of 101 V for a boundary-layer thickness of 0.06 m. For the same experiment Dolson and Biblarz[16] predict a boundary-layer drop of 110 V. Argyropoulos's results with the above results for the sheath, the formula would have the form

$$V=6.1+1700\delta, \tag{15}$$

where δ is measured in m and V in V.

Refernce 17 reports on the beneficial effect that increasing the seed fraction has on lowering electrode voltage drops. From the behavior of the electron collision cross sections with temperature,[10,18] the optimum conductivity is reached at seed fractions higher than in the core because of the lower local temperature at the electrodes. Heretofore, the only benefit would seem to be a higher boundary-layer conductivity, but as shown in Figs. 10–12, the local conductivity also affects the sheath drop. Hence, a higher value of σ_0 is expected to decrease the voltage loss associated with the sheath and ambipolar regions.

V. CONCLUSIONS AND RECOMMENDATIONS

This paper presents a computer analysis of the collisional sheath where magnetic field effects within the sheath are studied. A successful model of the sheath evolved from the assumption of steady state, frozen flow, and uniform temperature for the neutral and ion particles. Qualitatively, the results of the analysis used in this work offer much insight into voltage drops attributable to electrodes in contact with an MHD plasma. Quantitatively, these results are useful if it is remembered that the model is two dimensional and does not give the additional degree of freedom for current expansion afforded by three dimensions. A summary of the more basic conclusions which were drawn from the results is presented here.

(1) The sheath can be self-generated from a consistent set of equations with or without the use of an energy equation.

(2) The electrode boundary condition for charged particle density has little effect upon the field, while the insulated wall boundary condition has a profound effect.

(3) Current constrictions are necessary at the electrode to satisfy the system of equations.

(4) The resulting current-voltage diagram has a curvature consistent with predictions for space charge in a one-dimensional flow of current and with experimental evidence.

(5) The current density, for a given potential drop, varies inversely as the node spacing.

(6) The conductivity of the plasma within the sheath is critical in determining the sheath voltage drop, and methods to increase this conductivity will result in a decrease of both sheath and boundary-layer drops.

(7) Joule heating has little effect on the system as modeled because effects on electrode temperature are limited to a small region.

Other effects must be introduced to broaden the scope of this work. Neutral and ion heating may be incorporated into the model to investigate thermal instabilities known to exist for high Joule heating values[6]; conduction of heat in the solid walls may then be added. It is anticipated that some degree of frozen flow in the boundary layer would decrease its importance relative to the sheath drop. Also, by changing the sign of the charge at the electrode and introducing thermionic emission as a boundary condition, the cathode may be modeled.

The validity of these results is limited by the fact that the current density decreases in two dimensions rather than three. A three-dimensional scheme, admittedly a major task to develop, could render more realistic information on the effects of the sheath and on other electrode phenomena. One possible scheme is to model a three-dimensional system by using an axisymmetric cylindrical geometry for the point electrodes.

With each additional effect the model rises in complexity and the present numerical scheme will have to be adapted to the newer more powerful computing machines if more complete models are desired.

VI. LIST OF SYMBOLS

B magnetic field

D diffusion coefficient

e electron charge or exponential

J current density, conventional direction

J_e current density, electron contribution only

k Boltzmann's constant

L characteristic length

L_r characteristic recombination length

m particle mass

m_e electron mass

n particle density (i ions, e electrons)

n_0 characteristic charge density

p_0 pressure

Q_{en} collision cross section of electrons with species n

T temperature

T_e electron temperature

T_0 gas temperature in the sheath

x axial coordinate

y cross-channel coordinate

α coefficient $\epsilon_I/2kT_0$

β Hall parameter

γ Joule heating parameter

δ_s energy loss factor

ϵ_I seed ionization potential

ϵ_0 permittivity of a vacuum

θ temperature ratio T_e/T_0 or T/T_0

λ_s sheath thickness

μ mobility

ν collision frequency

σ conductivity

τ_r characteristic recombination time

ϕ electric potential

ϕ_0 characteristic voltage

ACKNOWLEDGMENT

This work is supported by the Air Force Office of Scientific Research.

*Present address: Naval Air Test Center, Patuxent River, Md. 20670.

[1]P.M. Chung, L. Talbot, and K.J. Touryan, AIAA J. 12, 144—153 (1974).

[2]S.H. Lam, AIAA J. 2, 256—262 (1964).

[3]C.H. Su and S.H. Lam, Phys. Fluids **6**, 1479 (1963).

[4]G.S. Argyropoulos, *et al.*, Thirteenth Symposium on Engineering Aspects of MHD, Stanford University, 1973 (unpublished).

[5]O. Biblarz, R.C. Dolson, and A.M. Shorb, J. Appl. Phys. **46**, 3343—3346 (1975).

[6]M.S.S. Hsu, Thirteenth Symposium on Engineering Aspects of MHD, Stanford University, 1973 (unpublished).

[7]R.L. Ketter and S.P. Prowell, *Modern Methods of Engineering Computation* (McGraw-Hill, New York, 1969), p. 84.

[8]S.J. Kline, *Similitude and Approximation Theory* (McGraw-Hill, New York, 1965, pp. 101—118.

[9]O. Biblarz and R.C. Dolson, Fourteenth Symposium on Engineering Aspects of MHD, UTSI, 1974, Tullahoma, Tenn. (unpublished).

[10]M. Mitchner and C.H. Kruger, *Partially Ionized Gases* (Wiley, New York, 1973), pp. 146—155; pp. 100—121.

[11]G.W. Sutton and A. Sherman, *Engineering Magnetohydrodynamics* (McGraw-Hill, New York, 1965), pp. 240—243.

[12]H.L. Langhaar, *Dimensional Analysis and Theory of Models* (Wiley, New York, 1951), pp. 29—38.

[13]J.D. Cobine, *Gaseous Conductors* (Dover, New York, 1958), p. 129.

[14]O.K. Sonju and J. Teno, Air Force Aero Propulsion Laboratory Report No. TR-74-47, Part 1, 1974, pp. 61—94 (unpublished).

[15]R. Kessler and R.H. Eustis, AIAA J. 9, 1640—1646 (1968).

[16]R.C. Dolson and O. Biblarz, Energy Convers. (to be published).

[17]C. Marston, E. Tate, and B. Zauderer, Sixth Inter. Conf. on MHD Ener. Power Gen., VIII, Washington, D.C., 1975 (unpublished).

[18]R.J. Rosa, *Magnetohydrodynamic Energy Conversion* (McGraw-Hill, New York, 1968), Chap. 2.